Enhanced intermodal four-wave mixing for visible and near-infrared wavelength generation in a photonic crystal fiber

Jinhui Yuan,[1,2,4,*] Xinzhu Sang,[1] Qiang Wu,[1,3] Guiyao Zhou,[4] Feng Li,[2] Xian Zhou,[2] Chongxiu Yu,[1] Kuiru Wang,[1] Binbin Yan,[1] Ying Han,[4] Hwa Yaw Tam,[2] and P. K. A. Wai[2]

[1]*State Key Laboratory of Information Photonics and Optical Communications (Beijing University of Posts and Telecommunications), P.O. Box 163 (BUPT), 100876 Beijing, China*

[2]*Photonics Research Center, Department of Electronic and Information Engineering, The Hong Kong Polytechnic University, Hung Hom, Kowloon, Hong Kong*

[3]*Department of Physics and Electrical Engineering, Northumbria University, Newcastle upon Tyne, NE1 8ST, UK*

[4]*Guangdong Provincial Key Laboratory of Nanophotonic Functional Materials and Devices, South China Normal University, 510006 Guangzhou, China*

**Corresponding author: yuanjinhui81@163.com*

Received January 28, 2015; accepted February 22, 2015;
posted February 26, 2015 (Doc. ID 233460); published March 23, 2015

We demonstrate experimentally an enhanced intermodal four-wave mixing (FWM) process through coupling positively chirped femtosecond pulses into the deeply normal dispersion region of the fundamental mode of an in-house fabricated photonic crystal fiber (PCF). In the intermodal phase-matching scheme, the energy of the pump waves at 800 nm in the fundamental mode is efficiently converted into the anti-Stokes waves around 553 nm and the Stokes waves within the wavelength range of 1445–1586 nm in the second-order mode. The maximum conversion efficiency of η_{as} and η_s of anti-Stokes and Stokes waves can be up to 21% and 16%, respectively. The Stokes frequency shift Ω is 5580 cm^{-1}. The fiber bending and intermodal walk-off effect of pulses do not have significant influence on the nonlinear optical process. © 2015 Optical Society of America

OCIS codes: (060.5295) Photonic crystal fibers; (190.4370) Nonlinear optics, fibers; (190.4380) Nonlinear optics, four-wave mixing.

http://dx.doi.org/10.1364/OL.40.001338

As a third-order parametric process, four-wave mixing (FWM) originates from the nonlinear response of bound electronics of a medium to the electromagnetic field. The nonlinear optical process can efficiently convert the pump energy into the blue-shifted anti-Stokes wave and red-shifted Stokes wave if the net energy and momentum are conserved during the interaction among the four optical waves. Since the first demonstration in a silica optical fiber in 1974 [1], the fiber-optic FWMs have attracted much attention, especially after the invention of photonic crystal fiber (PCF) [2,3], which is considered an ideal candidate for achieving FWM-based nonlinear frequency conversion of short pulses because of the enhanced nonlinearity and tailored dispersion.

Most of the previous works on fiber-optic FWMs refer to the generation of anti-Stokes and Stokes waves based on FWM in the same mode, fundamental or high-order modes, as the pump wave in PCFs with tens of centimeters length [4–7]. For the intramodal FWM, the dispersion profile of the PCFs needs to be appropriately designed, and the excitation wavelength of pump pulses has to be in the vicinity of zero dispersion wavelength of the propagation mode in order to satisfy the phase-matching condition. Thus, the flexibility in the PCF design and the choice of the existing laser sources to achieve the phase-matched FWM is limited. Moreover, when the pump pulses are located around the zero dispersion wavelength, other nonlinear optical effects such as modulation instability, intrapulse Raman scattering, and soliton fission will occur and interact to generate broad supercontinuum (SC), which not only can reduce the energy conversion from the pump to the anti-Stokes and Stokes waves, but also can severely contaminate the output optical spectra. Intermodal FWM can solve this problem of intramodal FWM. Intermodal FWM has been demonstrated in the initial nonlinear dynamics of SC generation in the multimode optical fibers [8,9] and PCFs [10,11]. For the intermodal FWM, when the pump wave is launched in the deeply normal or anomalous dispersion region of the fundamental mode, the anti-Stokes and Stokes waves can be generated based on the phase-matching condition fulfilled with other high-order modes. The intermodal nonlinear effects of short pulses in the multimode PCFs were studied theoretically by Poletti and Horak [12,13]. This PCF-based intermodal FWM scheme involving two pump photons in the fundamental mode and the anti-Stokes and Stokes photons in the high-order modes is a nonlinear frequency conversion technique. Tu *et al.* reported the energy conversion of femtosecond pulses around 800 nm to the anti-Stokes wave around 586 nm in a large mode area PCF, but the conversion efficiency is only 7%, and the nonlinear optical process is sensitive to the fiber bending [14].

In this Letter, an enhanced intermodal FWM is demonstrated experimentally in an air-silica PCF fabricated in-house. By the intermodal phase-matching scheme, two pump photons around 800 nm in the fundamental mode are efficiently converted into one anti-Stokes photon around 553 nm and one Stokes photon within the wavelength range of 1445–1586 nm in the second-order mode. The maximum conversion efficiency η_{as} and η_s of the anti-Stokes and Stokes waves can be up to 21% and 16%, respectively. The influences of fiber bending and walk-off

 © 2015 Optical Society of America

effect of pulses on the nonlinear optical process are also discussed.

The air-silica PCF used in the experiment has a core diameter of 5.9 μm and a relative hole size of 0.84, as shown in Fig. 1(a). Because of the large index difference between the core and cladding region, several guided modes can exist in this PCF. Here, we focused on the fundamental (1st) and the second-order (2nd) modes only. The effective refractive index curves calculated for the 1st and 2nd modes are presented in Fig. 1(b), and the corresponding spatial mode profiles calculated at 800 and 553 nm are shown in the insets 1 and 2 of Fig. 1(b), where most energy of these two modes is confined in the core region along with significant mode field overlap within the wavelength range of interest. Figure 1(c) shows the group-velocity dispersion profiles of the 1st and 2nd modes derived from the effective refractive index. The zero-dispersion wavelengths are located at 1049 and 950 nm, respectively. Thus, the PCF is pumped in the deeply normal dispersion region when femtosecond pulses at 800 nm are chosen as the pump wave. When the pump pulses at the center wavelength of 800 nm and average input power of 300 mW are launched into the PCF, the observed output far-field distributions of the residual pump and anti-Stokes wave are shown in insets 1 and 2 of Fig. 1(c), which are consistent with those shown in the insets 1 and 2 of Fig. 1(b).

In the experiment, the pump source used is a mode-locked Ti:sapphire laser with the center wavelength of 800 nm and pulse width of 120 fs. A positive chirp is introduced by a grating-based compressor. The initial pump pulses are elongated to 265 fs. The pump pulses are coupled by a 40× objective into a span of PCF with the length of 28 cm, and the coupling efficiency can be up to 65%. An isolator is used to prevent the output light from reflecting back into the laser cavity, and a variable attenuator is used to adjust the input average powers. The transmission loss is measured by the cut-back technique to be 1.1 dB/m at 800 nm. The output optical spectra are simultaneously monitored by two optical spectrum analyzers (Avaspec-256 and Avaspec-NIR-256) in the ranges of 200–1100 nm and 900–2500 nm, respectively.

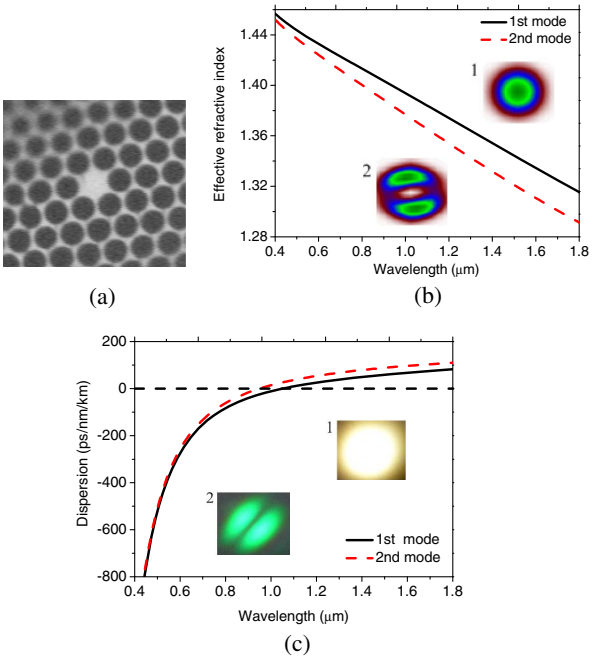

Fig. 1. (a) Cross-sectional structure of the PCF used in the experiment. (b) The effective refractive index profiles of the fundamental (1st) and second-order (2nd) modes. Insets 1 and 2 show the spatial mode profiles of 1st and 2nd modes calculated at 800 and 553 nm. (c) The group-velocity dispersion profiles calculated for 1st and 2nd modes. Insets 1 and 2 show the observed output far-field distributions of the pump and anti-Stokes wave for pump pulses at the center wavelength of 800 nm and the input average power of 300 mW.

For the intermodal FWM scheme, two fundamental pump photons generate one second-order anti-Stokes photon and one second-order Stokes photon. The phase matching refers to the contributions of silica material, waveguide structure, and nonlinearity. We can neglect the effect of nonlinearity because the positive-chirp introduced broadens the initial pump pulses and rapidly reduces the peak power [14]. Thus, the phase-mismatching factor $\delta\beta$ can be written as $\delta\beta = 2\beta_1(\omega_p) - \beta_2(\omega_p + \Omega) - \beta_2(\omega_p - \Omega)$, where $\beta_1(\omega_p)$, $\beta_2(\omega_p + \Omega)$, and $\beta_2(\omega_p - \Omega)$ are the propagation constants of the pump, anti-Stokes, and Stokes wave, respectively. The subscript 1 and 2 represent the 1st and 2nd modes, ω_p is the frequency of pump wave, and Ω is the Stokes frequency shift. In the energy conversion process, $\delta\beta = 0$ should be satisfied.

Figure 2(a) shows the $\delta\beta$ calculated without considering the nonlinearity contribution when the average input power P_{av} of the pump pulses at 800 nm is increased from 100 to 300 mW. We note that $\delta\beta$ reaches zero at the visible wavelength of 553.5 nm and near-infrared wavelength of 1446 nm. Because the center wavelength of pump pulses is located in the deeply normal dispersion region of the fundamental mode, the self-phase modulation (SPM) effect plays a dominate role. The initial spectra of the pump are broadened by SPM, and part of the pump energy is depleted. Figure 2(b) shows the observed output spectra from the PCF. The inset shows the zoom-in spectra of the anti-Stokes waves. It can be seen that the anti-Stokes waves and the weaker Stokes waves with gradually enhanced powers are generated at an approximate Ω of 5580 cm^{-1}, corresponding to the visible wavelength of 553.1 nm and near-infrared wavelength of 1445 nm, which agrees well with the calculation results of Fig. 2(a). Also, as seen from the far-field distributions shown in the insets 1 and 2 of Fig. 1(c), the pump and anti-Stokes waves propagate in the fundamental and second-order modes, respectively. Because of dispersion and nonlinearity characteristics in different dispersion regions, the output spectra of visible anti-Stokes waves and near-infrared Stokes waves are broadened. For the Stokes waves located in the anomalous dispersion region of second-order mode, the significant spectral broadening is induced by the soliton-related nonlinear optical process. Figure 2(c) shows the dependences of the output anti-Stokes and Stokes wave power P_{as} and P_s and the conversion efficiency η_{as} and η_s from the incident pump to spectrally isolated anti-Stokes and Stokes waves on P_{av}. As seen from Fig. 2(c), for the coupling efficiency of 65%, P_{as} are measured to be 4.55, 16.9,

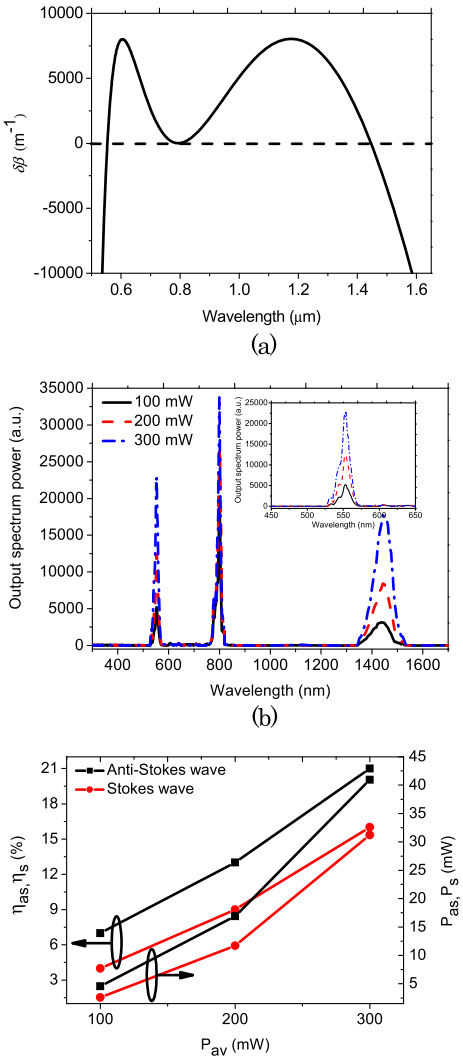

Fig. 2. (a) Phase-mismatch factor $\delta\beta$ calculated for the pump wave at 800 nm and average input power P_{av} of 100, 200, and 300 mW. (b) The observed output spectra. The inset shows the zoom-in spectra of the anti-Stokes waves. (c) The dependences of the output anti-Stokes and Stokes wave power P_{as} and P_s and the conversion efficiency η_{as} and η_s on P_{av}.

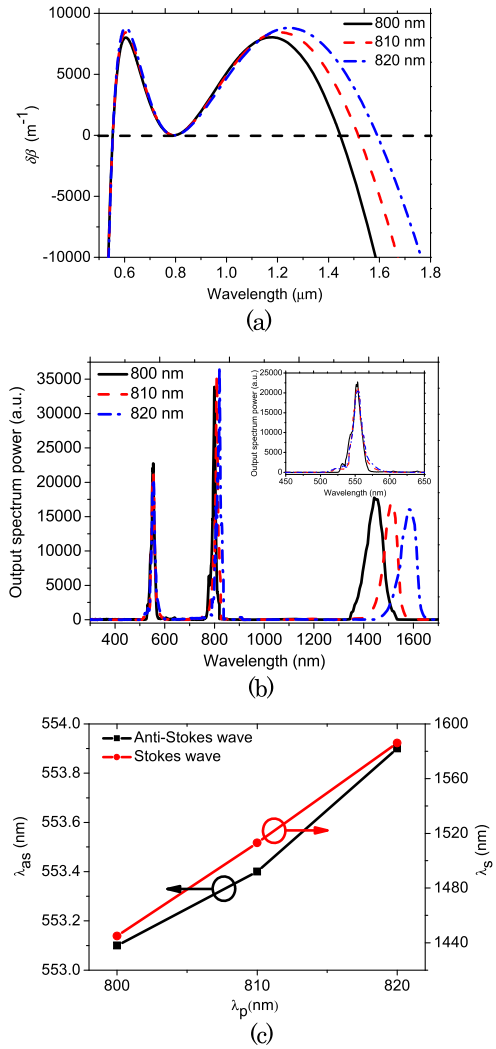

Fig. 3. (a) Phase-mismatch factor $\delta\beta$ calculated for the average input power $P_{\text{av}} = 300$ mW and the center wavelength λ_p of pump pulses at 800, 810, and 820 nm. (b) The observed output spectra. The inset shows the zoom-in spectra of the anti-Stokes waves. (c) The dependences of the center wavelength λ_{as} and λ_s of the anti-Stokes and Stokes wave on λ_p on the pump wavelength.

and 40.95 mW, and P_s are measured to be 2.6, 11.7, and 31.2 mW for $P_{\text{av}} = 100$, 200, and 300 mW, respectively. The corresponding η_{as} increases from 7% to 13%, and to 21%, and η_s increases from 4% to 9%, and to 16%, when P_{av} increases from 100, to 200, and to 300 mW, respectively. The maximum η_{as} and η_s can be up to 21% and 16%, which are mainly attributed to strong intermodal nonlinearity induced by the significant mode field overlap between the fundamental and second-order modes during the propagation. Thus, the anti-Stokes and Stokes waves without SC contamination are efficiently generated through this intermodal FWM process.

When the center wavelength λ_p of pump pulses at P_{av} of 300 mW is adjusted from 800 to 810, and to 820 nm, similar intermodal FWM process occurs. As shown in Fig. 3(a), the calculated $\delta\beta$ reaches zero at the wavelengths of 553.5 nm, 553.6 nm, and 553.8 nm, and 1446 nm, 1516 nm, and 1591 nm, respectively. Figure 3(b) and the inset show the observed whole output spectra and the zoom-in spectra of the anti-Stokes waves. Figure 3(c) shows the dependences of the center wavelength λ_{as} and λ_s of the anti-Stokes and Stokes waves on λ_p. As seen from Fig. 3(c), the λ_{as} are centered at 553.1 nm, 553.4 nm, and 553.9 nm, and λ_s are centered at 1445 nm, 1513 nm, and 1586 nm, respectively, which correspond to the approximate Ω of 5580, 5724, and 5859 cm^{-1}. It can be seen from both of the theoretical and experimental results that λ_{as} is insensitive to the pump wavelength λ_p when compared to λ_s, which is obviously different from the results demonstrated in intramode FWM. Thus, nearly constant-wavelength anti-Stokes waves and widely tunable Stokes waves can be generated, and the spectral power density of the anti-Stokes waves can be much higher than that of the Stokes waves because of the different spectral bandwidths. As λ_p is increased, the decreasing energy conversion is considered to be due to increased pulse walk-off and reduced mode field overlap.

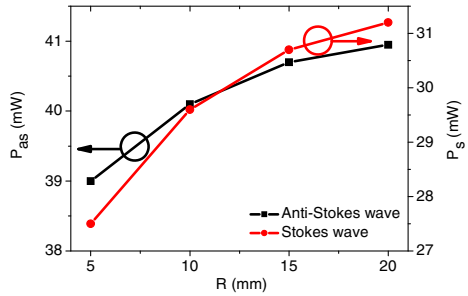

Fig. 4. Dependences of the output anti-Stokes and Stokes wave power P_{as} and P_s measured at the pump center wavelength λ_p of 800 nm and the average input power P_{av} of 300 mW on the fiber bending radius R.

In the following, we will discuss the influences of the effects of fiber bending and pulse walk-off. As reported in [14], the intermodal FWM process can be completely suppressed by the fiber bending at the entrance end because of its dependence on the spontaneous buildup of the Stokes wave, which propagates in the second-order mode and has a large leaky loss owing to the small relative hole size in the cladding. In contrast, our PCF has a large relative hole size, so the leaky loss of the Stokes wave in the second-order mode induced by the fiber bending is greatly reduced. As shown in Fig. 4, when the fiber bending radius R at the entrance end is reduced from 20 to 15, to 10, and to 5 mm, P_{as} changes from 40.95 to 40.7, to 40.1, and to 39 mW, and P_s changes from 31.2 to 30.7, to 29.6, and to 27.5 mW, respectively, for λ_p at 800 nm and P_{av} at 300 mW. The experimental results indicate that the energy conversion process based on this intermodal FWM is insensitive to the fiber bending even if R is as small as 5 mm.

The intermodal walk-off effect between the pump and anti-Stokes and Stokes pulses can be described by the walk-off parameter $d_{12} = 1/v_g^{(1)}(\lambda_p) - 1/v_g^{(2)}(\lambda_p)$, where $v_g^{(1)}(\lambda_p)$ and $v_g^{(2)}(\lambda_p)$ are the group velocities of the 1st and 2nd modes at λ_p. The calculated d_{12} at λ_p of 800, 810, and 820 nm are the order of $\sim 10^{-2}$ ps/mm. Moreover, the positive chirp can speed up the pump pulse broadening. Therefore, the intermodal FWM effects can noticeably occur because of the longer walk-off length in our PCF.

In summary, an enhanced intermodal FWM process is demonstrated through pumping in the deeply normal dispersion region of the fundamental mode of a PCF. By intermodal phase-matching between the fundamental and second-order modes, nearly constant-wavelength visible anti-Stokes waves and widely tunable near-infrared Stokes waves are generated. Moreover, the fiber bending and intermodal walk-off effect of pulses do not have significant influence on the nonlinear optical process. This intermodal FWM scheme can be used to generate the visible and near-infrared short pulse sources without SC contamination for ultrafast photonics and spectroscopy, biomedical optics, and multi-photon ionization.

This work is partly supported by the National Natural Science Foundation of China (61307109 and 61475023), the Beijing Natural Science Foundation (4152037), the National High-Technology Research and Development Program of China (2013AA031501), the Specialized Research Fund for the Doctoral Program of Higher Education (20120005120021), the Fundamental Research Funds for the Central Universities (2013RC1202), the Fund of State Key Laboratory of Information Photonics and Optical Communications (BUPT) of China, the Hong Kong Scholars Program 2013 (PolyU G-YZ45), and the Research Grant Council of the Hong Kong Special Administrative Region China (PolyU5272/12E).

References

1. R. H. Stolen, J. E. Bjorkholm, and A. Ashkin, Appl. Phys. Lett. **24**, 308 (1974).
2. P. S. J. Russell, Science **299**, 358 (2003).
3. J. C. Knight, Nature **424**, 847 (2003).
4. A. V. Husakou and J. Herrmann, Appl. Phys. Lett. **83**, 3867 (2003).
5. D. A. Akimov, E. E. Serebryannikov, A. M. Zheltikov, M. Schmitt, R. Maksimenka, W. Kiefer, K. V. Dukel'skii, V. S. Shevandin, and Y. N. Kondrat'ev, Opt. Lett. **28**, 1948 (2003).
6. D. Nodop, C. Jauregui, D. Schimpf, J. Limpert, and A. Tünnermann, Opt. Lett. **34**, 3499 (2009).
7. A. Herzog, A. Shamir, and A. A. Ishaaya, Opt. Lett. **37**, 82 (2012).
8. A. Mussot, T. Sylvestre, L. Provino, and H. Maillotte, Opt. Lett. **28**, 1820 (2003).
9. J. Cheng, M. E. V. Pedersen, K. Charan, K. Wang, C. Xu, L. Grüner-Nielsen, and D. Jakobsen, Appl. Phys. Lett. **101**, 161106 (2012).
10. C. Lesvigne, V. Couderc, A. Tonello, P. Leproux, A. Barthélémy, S. Lacroix, F. Druon, P. Blandin, M. Hanna, and P. Georges, Opt. Lett. **32**, 2173 (2007).
11. T. Sylvestre, A. R. Ragueh, M. W. Lee, B. Stiller, G. Fanjoux, B. Barviau, A. Mussot, and A. Kudlinski, Opt. Lett. **37**, 130 (2012).
12. F. Poletti and P. Horak, J. Opt. Soc. Am. B **25**, 1645 (2008).
13. F. Poletti and P. Horak, Opt. Express **17**, 6134 (2009).
14. H. Tu, Z. Jiang, D. L. Marks, and S. A. Boppart, Appl. Phys. Lett. **94**, 101109 (2009).